

Airplane Design with Aerodynamic Shape Optimization

Antony Jameson¹

¹Thomas V. Jones Professor of Engineering
Aeronautics & Astronautics Department, Stanford University

ASSISTED BY KUI OU

June, 2010

SHANGHAI.上海

Table of Contents I

- 1 Aerodynamic Design
 - Multidisciplinary Tradeoffs
 - Airplane Design Process
- 2 Aerodynamic Shape Optimization
 - Control Theory
- 3 Design Process
 - Design Process Outline
- 4 Applications of Aerodynamic Shape Optimization
- 5 Appendix
 - Appendix A - Biography of Antony Jameson
 - Appendix B - CFD Applications at Boeing and Airbus
 - Appendix C - FLO and SYN Codes and Their Usages
 - Appendix D - Mathematics of Adjoint Based Shape Optimization

AERODYNAMIC DESIGN

Aerodynamic Design Tradeoffs

A good first estimate of performance is provided by the Breguet range equation:

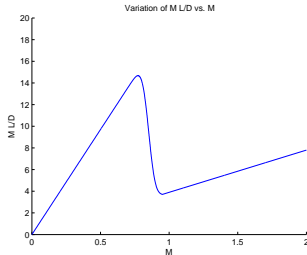
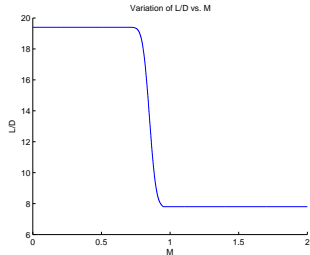
$$\text{Range} = \frac{VL}{D} \frac{1}{SFC} \log \frac{W_0 + W_f}{W_0}. \quad (1)$$

Here V is the speed, L/D is the lift to drag ratio, SFC is the specific fuel consumption of the engines, W_0 is the loading weight (empty weight + payload + fuel resourced), and W_f is the weight of fuel burnt.

Equation (1) displays the multidisciplinary nature of design.

A light structure is needed to reduce W_0 . SFC is the province of the engine manufacturers. The aerodynamic designer should try to maximize $\frac{VL}{D}$. This means the cruising speed V should be increased until the onset of drag rise at a Mach Number $M = \frac{V}{c} \sim .85$. But the designer must also consider the impact of shape modifications in structure weight.

Aerodynamic Efficiency of Long Range Transport Aircraft



Aerodynamic Design Tradeoffs

The drag coefficient can be split into an approximate fixed component C_{D_0} , and the induced drag due to lift.

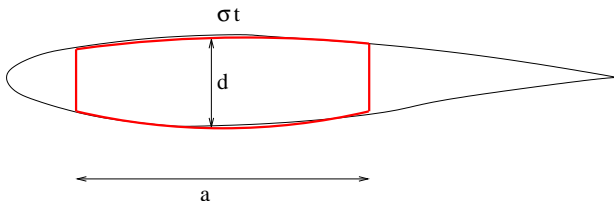
$$C_D = C_{D_0} + \frac{C_L^2}{\pi \epsilon AR} \quad (2)$$

where AR is the aspect ratio, and ϵ is an efficiency factor close to unity. C_{D_0} includes contributions such as friction and form drag. It can be seen from this equation that L/D is maximized by flying at a lift coefficient such that the two terms are equal, so that the induced drag is half the total drag. Moreover, the actual drag due to lift

$$D_v = \frac{2L^2}{\pi \epsilon \rho V^2 b^2}$$

varies inversely with the square of the span b . Thus there is a direct conflict between reducing the drag by increasing the span and reducing the structure weight by decreasing it.

Weight Tradeoffs



The bending moment M is carried largely by the upper and lower skin of the wing structure box. Thus

$$M = \sigma t d a$$

For a given stress σ , the required skin thickness varies inversely as the wing depth d . Thus weight can be reduced by increasing the thickness to chord ratio. But this will increase shock drag in the transonic region.

15–30 engineers
1.5 years
\$6–12 million

**Conceptual
Design**

Defines Mission
Preliminary sizing
Weight, performance

100–300 engineers
2.5 years
\$60–120 million

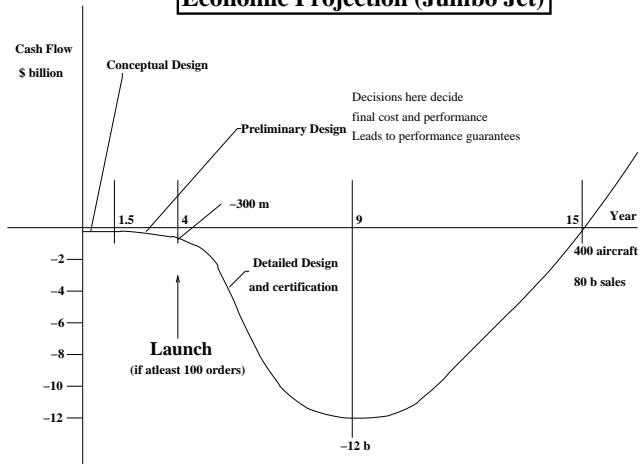
**Preliminary
Design**

6000 engineers
5 years
\$3–12 billion

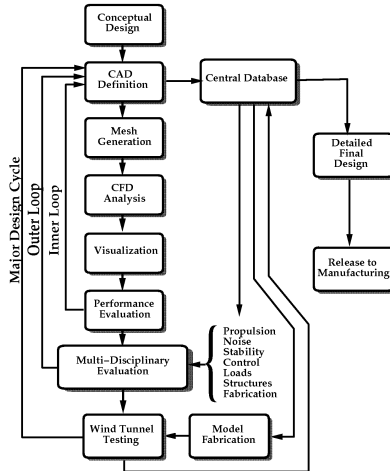
Final Design

Cash Flow

Economic Projection (Jumbo Jet)



Aerodynamic Design



AERODYNAMIC SHAPE OPTIMIZATION USING CONTROL THEORY

Control Theory Approach to Design

A wing is a device to control the flow. Apply the theory of control of partial differential equations (J.L.Lions) in conjunction with CFD.

References

- Pironneau (1964) Optimum shape design for subsonic potential flow
- Jameson (1988) Optimum shape design for transonic and supersonic flow modeled by the transonic potential flow equation and the Euler equations

Control Theory Approach to the Design Method

Define a cost function

$$I = \frac{1}{2} \int_{\mathcal{B}} (p - p_t)^2 d\mathcal{B}$$

or

$$I = \frac{1}{2} \int_{\mathcal{B}} (q - q_t)^2 d\mathcal{B}$$

The surface shape is now treated as the control, which is to be varied to minimize I , subject to the constraint that the flow equations are satisfied in the domain D .

Choice of Domain

ALTERNATIVES

- 1 Variable computational domain - Free boundary problem
- 2 Transformation to a fixed computational domain - Control via the transformation function

EXAMPLES

- 1 2D via Conformal mapping with potential flow
- 2 2D via Conformal mapping with Euler equations
- 3 3D Sheared Parabolic Coordinates with Euler equation
- 4 ...

Formulation of the Control Problem

Suppose that the surface of the body is expressed by an equation

$$f(\underline{x}) = 0$$

Vary f to $f + \delta f$ and find δI .

If we can express

$$\delta I = \int_{\mathcal{B}} g \delta f d\mathcal{B} = (g, \delta f)_{\mathcal{B}}$$

Then we can recognize g as the gradient $\frac{\partial I}{\partial f}$.

Choose a modification

$$\delta f = -\lambda g$$

Then to first order

$$\delta I = -\lambda (g, g)_{\mathcal{B}} \leq 0$$

In the presence of constraints project g into the admissible trial space.

Accelerate by the conjugate gradient method.

Traditional Approach to Design Optimization

Define the geometry through a set of design parameters, for example, to be the weights α_i applied to a set of shape functions $b_i(x)$ so that the shape is represented as

$$f(x) = \sum \alpha_i b_i(x).$$

Then a cost function I is selected, for example, to be the drag coefficient or the lift to drag ratio, and I is regarded as a function of the parameters α_i . The sensitivities $\frac{\partial I}{\partial \alpha_i}$ may be estimated by making a small variation $\delta \alpha_i$ in each design parameter in turn and recalculating the flow to obtain the change in I . Then

$$\frac{\partial I}{\partial \alpha_i} \approx \frac{I(\alpha_i + \delta \alpha_i) - I(\alpha_i)}{\delta \alpha_i}.$$

The gradient vector $\mathcal{G} = \frac{\partial I}{\partial \alpha}$ may now be used to determine a direction of improvement. The simplest procedure is to make a step in the negative gradient direction by setting

$$\alpha^{n+1} = \alpha^n + \delta \alpha,$$

where

$$\delta \alpha = -\lambda \mathcal{G}$$

so that to first order

$$I + \delta I = I - \mathcal{G}^T \delta \alpha = I - \lambda \mathcal{G}^T \mathcal{G} < I$$

Disadvantages

The main disadvantage of this approach is the need for a number of flow calculations proportional to the number of design variables to estimate the gradient. The computational costs can thus become prohibitive as the number of design variables is increased.

Formulation of the Adjoint Approach to Optimal Design

For flow about an airfoil or wing, the aerodynamic properties which define the cost function are functions of the flow-field variables (w) and the physical location of the boundary, which may be represented by the function \mathcal{F} , say. Then

$$I = I(w, \mathcal{F}),$$

and a change in \mathcal{F} results in a change

$$\delta I = \left[\frac{\partial I^T}{\partial w} \right] \delta w + \left[\frac{\partial I^T}{\partial \mathcal{F}} \right] \delta \mathcal{F} \quad (3)$$

in the cost function. Suppose that the governing equation R which expresses the dependence of w and \mathcal{F} within the flowfield domain D can be written as

$$R(w, \mathcal{F}) = 0. \quad (4)$$

Then δw is determined from the equation

$$\delta R = \left[\frac{\partial R}{\partial w} \right] \delta w + \left[\frac{\partial R}{\partial \mathcal{F}} \right] \delta \mathcal{F} = 0. \quad (5)$$

Since the variation δR is zero, it can be multiplied by a Lagrange Multiplier ψ and subtracted from the variation δI without changing the result.

Formulation of the Adjoint Approach to Optimal Design

$$\begin{aligned} \delta I &= \frac{\partial I^T}{\partial w} \delta w + \frac{\partial I^T}{\partial \mathcal{F}} \delta \mathcal{F} - \psi^T \left(\left[\frac{\partial R}{\partial w} \right] \delta w + \left[\frac{\partial R}{\partial \mathcal{F}} \right] \delta \mathcal{F} \right) \\ &= \left\{ \frac{\partial I^T}{\partial w} - \psi^T \left[\frac{\partial R}{\partial w} \right] \right\} \delta w + \left\{ \frac{\partial I^T}{\partial \mathcal{F}} - \psi^T \left[\frac{\partial R}{\partial \mathcal{F}} \right] \right\} \delta \mathcal{F}. \end{aligned} \quad (6)$$

Choosing ψ to satisfy the adjoint equation

$$\left[\frac{\partial R}{\partial w} \right]^T \psi = \frac{\partial I}{\partial w} \quad (7)$$

the first term is eliminated, and we find that

$$\delta I = \mathcal{G}^T \delta \mathcal{F}, \quad (8)$$

where

$$\mathcal{G} = \frac{\partial I^T}{\partial \mathcal{F}} - \psi^T \left[\frac{\partial R}{\partial \mathcal{F}} \right].$$

An improvement can be made with a shape change

$$\delta \mathcal{F} = -\lambda \mathcal{G}$$

where λ is positive and small enough that the first variation is an accurate estimate of δI .

Advantages

- The advantage is that (8) is independent of δw , with the result that the gradient of I with respect to an arbitrary number of design variables can be determined without the need for additional flow-field evaluations.
- The cost of solving the adjoint equation is comparable to that of solving the flow equations. Thus the gradient can be determined with roughly the computational costs of two flow solutions, independently of the number of design variables, which may be infinite if the boundary is regarded as a free surface.
- When the number of design variables becomes large, the computational efficiency of the control theory approach over traditional approach, which requires direct evaluation of the gradients by individually varying each design variable and recomputing the flow fields, becomes compelling.

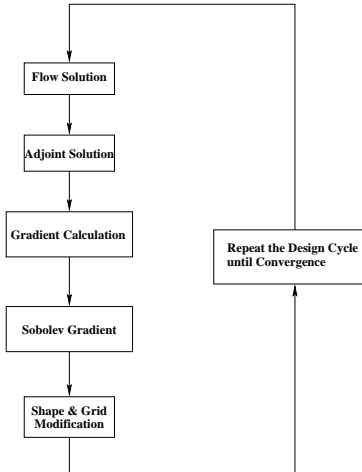
OUTLINE OF THE DESIGN PROCESS

Outline of the Design Process

The design procedure can finally be summarized as follows:

- 1 Solve the flow equations for ρ , u_1 , u_2 , u_3 and p .
- 2 Solve the adjoint equations for ψ subject to appropriate boundary conditions.
- 3 Evaluate \mathcal{G} and calculate the corresponding Sobolev gradient $\overline{\mathcal{G}}$.
- 4 Project $\overline{\mathcal{G}}$ into an allowable subspace that satisfies any geometric constraints.
- 5 Update the shape based on the direction of steepest descent.
- 6 Return to 1 until convergence is reached.

Design Cycle



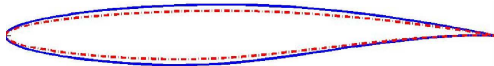
Constraints

- Fixed C_L .
- Fixed span load distribution to prevent too large C_L on the outboard wing which can lower the buffet margin.
- Fixed wing thickness to prevent an increase in structure weight.
 - Design changes can be limited to a specific spanwise range of the wing.
 - Section changes can be limited to a specific chordwise range.



- Smooth curvature variations via the use of Sobolev gradient.

Application of Thickness Constraints



- Prevent shape change penetrating a specified skeleton (colored in red).
- Separate thickness and camber allow free camber variations.
- Minimal user input needed.

APPLICATIONS OF SHAPE OPTIMIZATION

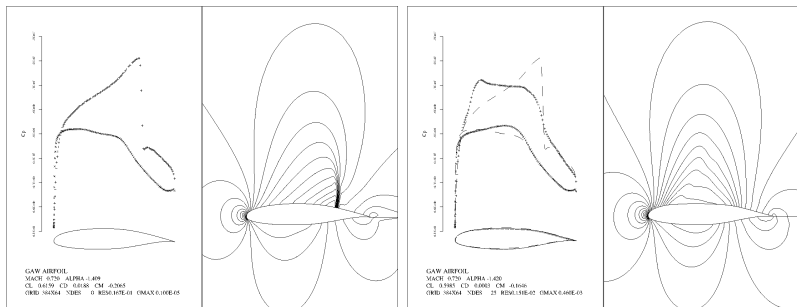
SHOCK FREE AIRFOIL DESIGN

Shock Free Airfoil Design

- The search for profiles which give shock free transonic flows was the subject of intensive study in the 1965–70 period.
- Morawetz' theorem (1954) states that a shock free transonic flow is an isolated point. Any small perturbation in Mach number, angle of attack, or shape causes a shock to appear in the flow.
- Nieuwland generated shock free profiles by developing solutions in the hodograph plane. The most successful method was that developed by Garabedian and his co-workers. This used complex characteristics to develop solution in the hodograph plane, which was then mapped to the physical plane. It was hard to find hodograph solutions which mapped to physical realizable closed profiles. It generally took one or two months to produce an acceptable solution.
- By using shape optimization to minimize the drag coefficient at a fixed lift, shock free solutions can be found in less than one minute.

Two Dimensional Studies of Transonic Airfoil Design

Pressure distribution and Mach contours for the GAW airfoil

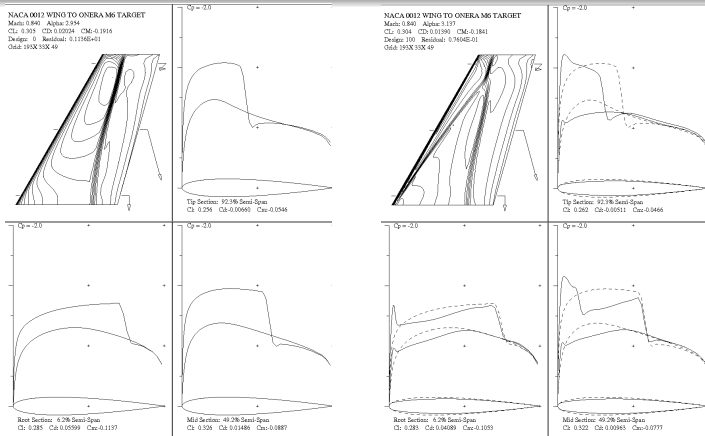


(a) Before the redesign

(b) After the redesign

INVERSE WING DESIGN

NACA 0012 WING TO ONERA M6 TARGET

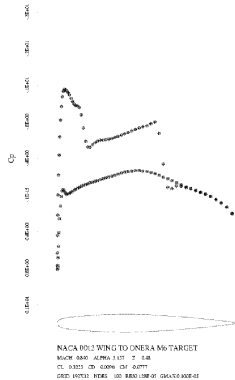
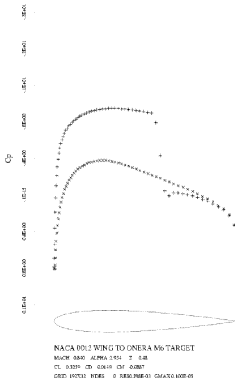


(c) Starting wing: NACA 0012

(d) Target wing: ONERA M6

This is a difficult problem because of the presence of the shock wave in the target pressure and because the profile to be recovered is symmetric while the target pressure is not

Pressure Profile at 48% Span



(e) Starting wing: NACA 0012

(f) Target wing: ONERA M6

The pressure distribution of the final design match the specified target, even inside the shock.

REDESIGN OF BOEING 747 - SUPER B747

Planform and Aero-Structural Optimization

The shape changes in the section needed to improve the transonic wing design are quite small. However, in order to obtain a true optimum design larger scale changes such as changes in the wing planform (sweepback, span, chord, and taper) should be considered. Because these directly affect the structure weight, a meaningful result can only be obtained by considering a cost function that takes account of both the aerodynamic characteristics and the weight.

Consider a cost function is defined as

$$I = \alpha_1 C_D + \alpha_2 \frac{1}{2} \int_B (p - p_d)^2 dS + \alpha_3 C_W$$

Maximizing the range of an aircraft provides a guide to the values for α_1 and α_3 .

Choice of Weighting Constants

The simplified Breguet range equation can be expressed as

$$R = \frac{V}{C} \frac{L}{D} \log \frac{W_1}{W_2}$$

where W_2 is the empty weight of the aircraft.

With fixed V/C , W_1 , and L , the variation of R can be stated as

$$\frac{\delta R}{R} = - \left(\frac{\delta C_D}{C_D} + \frac{1}{\log \frac{W_1}{W_2}} \frac{\delta W_2}{W_2} \right) = - \left(\frac{\delta C_D}{C_D} + \frac{1}{\log \frac{C_{W1}}{C_{W2}}} \frac{\delta C_{W2}}{C_{W2}} \right).$$

Therefore minimizing

$$I = C_D + \alpha C_W,$$

by choosing

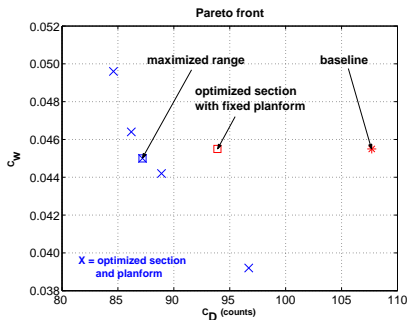
$$\alpha = \frac{C_D}{C_{W2} \log \frac{C_{W1}}{C_{W2}}},$$

corresponds to maximizing the range of the aircraft.

Boeing 747 Euler Planform Results: Pareto Front

Test case: Boeing 747 wing–fuselage and modified geometries at the following flow conditions.

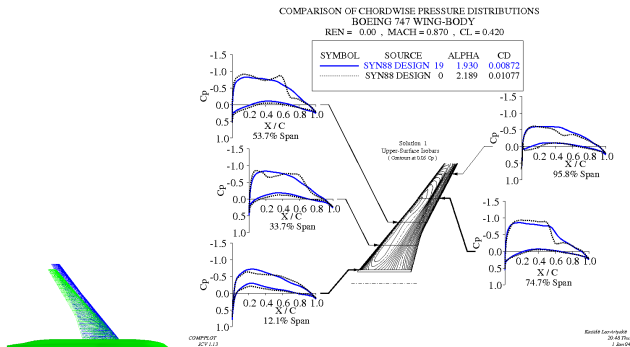
$$M_\infty = 0.87, \quad C_L = 0.42 \text{ (fixed)}, \quad \text{multiple } \frac{\alpha_3}{\alpha_1}$$



Boeing 747 Euler Planform Results: Sweepback, Span, Chord, and Section Variations to Maximize Range

Geometry	Baseline	Optimized	Variation (%)
Sweep ($^{\circ}$)	42.1	38.8	-7.8
Span (ft)	212.4	226.7	+6.7
C_{root}	48.1	48.6	+1.0
C_{mid}	30.6	30.8	+0.7
C_{tip}	10.78	10.75	+0.3
t_{root}	58.2	62.4	+7.2
t_{mid}	23.7	23.8	+0.4
t_{tip}	12.98	12.8	-0.8

Boeing 747 Euler Planform Results: Sweepback, Span, Chord, and Section Variations to Maximize Range



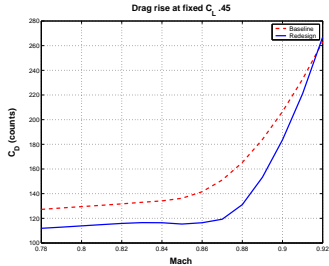
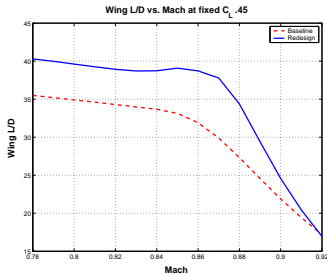
- C_D is reduced from 107.7 drag counts to 87.2 drag counts (19%).
- C_W is reduced from 0.0455 (69,970 lbs) to 0.0450 (69,201 lbs) (1.1%).

Super B747 V. 6



- Design a new wing for Boeing 747.
- Strategy
 - Use the 747 fuselage.
 - Use a new planform (from the planform optimization result).
 - Use new airfoil section (AJ airfoils).
 - Optimized for fixed lift coefficient at four Mach numbers: 0.78, 0.85, 0.86 and 0.87.

Drag Rise and Wing L/D of Super B757 V. 6



- : Baseline
- : Redesign

Comparison Between Boeing 747 and Super B747 V. 6

	C_L	C_D (counts)	C_W (counts)
Boeing	0.45	141.3 (107.0 pressure. 34.3 viscous)	499 (82,550 lbs)
Super B747	0.50	138.3 (99.2 pressure. 39.1 viscous)	475 (78,640 lbs)

LOWER DRAG AND LIGHTER WING WEIGHT AT HIGHER C_L

WING REDESIGN FOR THE FASTEST P51 RENO RACER

P51 Racer



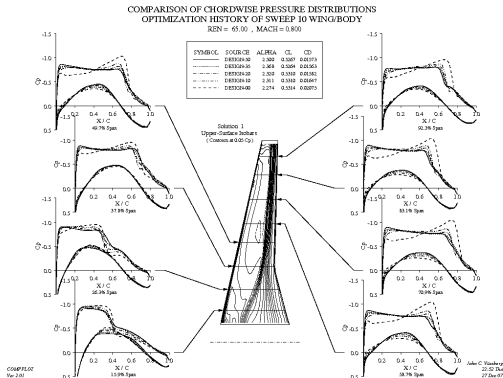
- Aircraft competing in the Reno Air Races reach speeds above 500 MPH, encountering compressibility drag due to the appearance of shock waves.
- Objective is to delay drag rise without altering the wing structure. Hence try adding a bump on the wing surface.

WING DESIGN WITH REDUCED SWEEP

Background for Studies of Reduced Sweep

- Current Transonic Transports
 - Cruise Mach: $0.76 \leq M \leq 0.86$
 - C/4 Sweep: $25^\circ \leq \Lambda \leq 35^\circ$
 - Wing Planform Layout Knowledge Base
 - Heavily Influenced By *Design Charts*
 - Data Developed From *Cut-n-Try* Designs
 - Data Augmented With Parametric Variations
 - Data Collected Over The Years
 - Includes Shifts Due To Technologies
e.g., Supercritical Airfoils, Composites, etc.

Pure Aerodynamic Optimizations



Evolution of Pressures for $\Lambda = 10^\circ$ Wing during Optimization

Pure Aerodynamic Optimizations

Mach	Sweep	C_L	C_D	$C_{D.tot}$	ML/D	$\sqrt{ML/D}$
0.85	35°	0.500	153.7	293.7	14.47	15.70
0.84	30°	0.510	151.2	291.2	14.71	16.05
0.83	25°	0.515	151.2	291.2	14.68	16.11
0.82	20°	0.520	151.7	291.7	14.62	16.14
0.81	15°	0.525	152.4	292.4	14.54	16.16
0.80	10°	0.530	152.2	292.2	14.51	16.22
0.79	5°	0.535	152.5	292.5	14.45	16.26

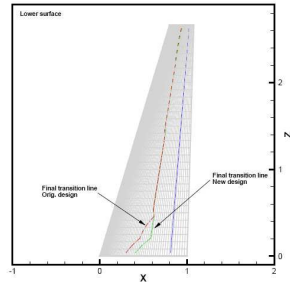
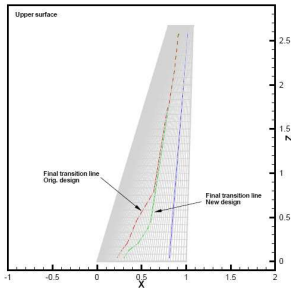
- C_D in counts
- $C_{D.tot} = C_D + 140$ counts
- Lowest Sweep Favors $\sqrt{ML/D} \simeq 4.0\%$

Conclusion of Swept Wing Study

- An unswept wing at Mach 0.80 offers slightly better range efficiency than a swept wing at Mach 0.85.
- It would also improve TO, climb, descent and landing.
- Perhaps B737/A320 replacements should have unswept wings.

WING DESIGN WITH NATURAL LAMINAR FLOW

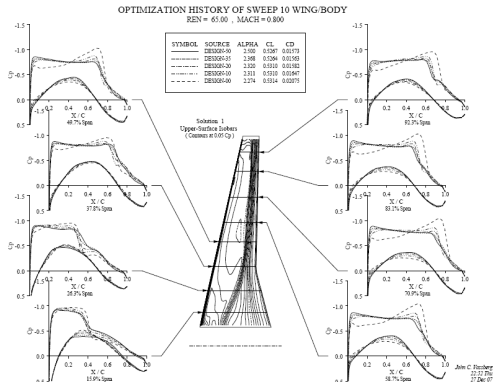
Automatic transition prediction design for NLF 3D wing



- initial
- - - final, original design
- - - final, new design

Low sweep is needed for natural laminar flow (NLF)

Low sweep wings can be designed for Mach 0.8



DESIGN FOR FLIGHT AT MACH 1

Flight at mach 1

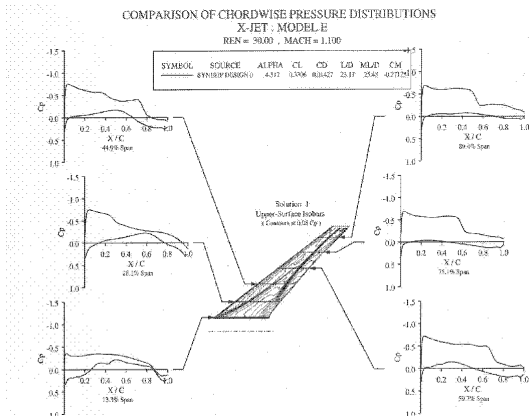
It appears possible to design a wing with very low drag at Mach 1, as indicated in the table below:

C_L	$C_{D_{pres}}$ (counts)	$C_{D_{friction}}$ (counts)	$C_{D_{wing}}$ (counts)
0.300	47.6	41.3	88.9
0.330	65.6	40.8	106.5

- The data is for a wing-fuselage combination, with engines mounted on the rear fuselage simulated by bumps.
- The wing has 50 degrees of sweep at the leading edge, and the thickness to chord ratio varies from 10 percent at the root to 7 percent at the tip.
- To delay drag rise to Mach one requires fuselage shaping in conjunction with wing optimization.

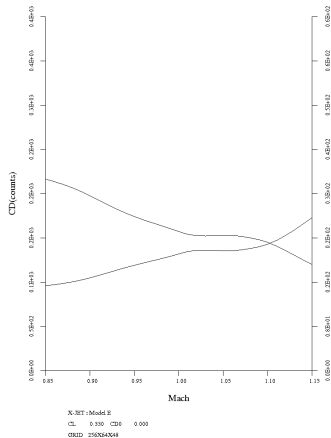
X Jet: Model E

Pressure Distribution on the Wing at Mach 1.1



X Jet: Model E

Drag Rise



GULFSTREAM G650 WING AND TAIL DESIGN

Gulfstream G650 3 Views



Gulfstream G650 Wind Tunnel Testing



- Aerodynamic wing and tail design in collaboration with Bob Mills using Syn107

Gulfstream G650 Design Work by Antony Jameson



- Calculations performed at IAI (Intelligent Aerodynamic Inc), 845 Sharon Park Drive, Menlo Park, CA.
- Both wing and tail sections optimized for multiple flight conditions

Gulfstream G650 Performance



- 7000nm at Mach 0.85
- Trans Pacific at Mach 0.90
- Drag divergence Mach number 0.88
- Max operating Mach No. 0.925 (0.92 for Cessna Citation 10)

Gulfstream G650 Flight Test

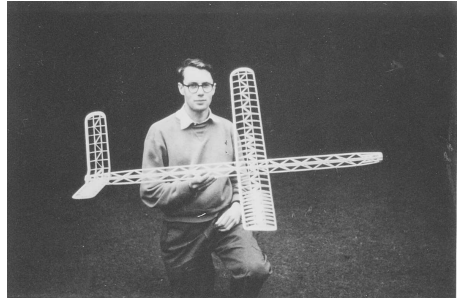


- Flight tests ongoing since Nov 2009
- Flight tests confirmed performance estimates

THANKS AND QUESTIONS

BIOGRAPHY OF ANTONY JAMESON

Cambridge University



- Studied engineering at Trinity Hall, Cambridge University, graduating with first class honors in 1958.
- Stayed on at Cambridge to obtain a Ph.D. in Magneto hydrodynamics,
- Became a Research Fellow of Trinity Hall from 1960-1963.

CAMBRIDGE UNIVERSITY 1955-1962

- 1962 Alfred P. Sloan Foreign Post-Doctoral Fellow, Massachusetts Institute of Technology
- 1958 Master of Arts in Engineering, First Class Honors, Cambridge University
- 1955 Open Scholarship to Trinity Hall, Cambridge

New York University, Courant Institute

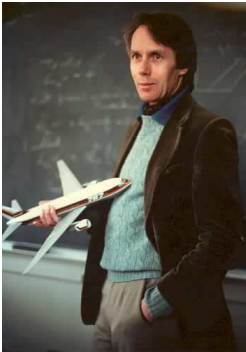


- Senior Research Scientist, 1972-1974
- Associate Professor of Mathematics, 1973
- Professor of Computer Science, 1974-1980

NEW YORK UNIVERSITY 1972-1980

- 1980 NASA Medal for Exeptional Scientific Achievement

Princeton University

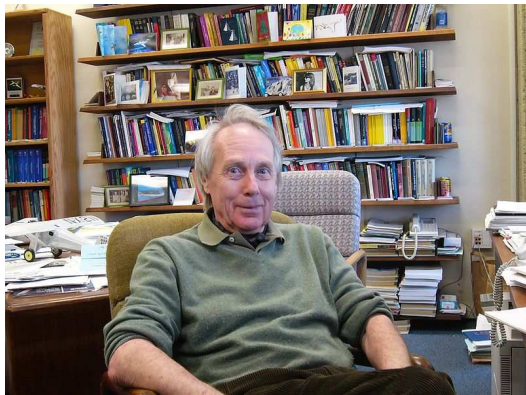


- Professor of Mech. and Aero. Engineering, 1980-1982
- Director, Program in Applied and Comp. Maths, 1986-1988
- James S. McDonnell Distinguished University Professor, 1982-1997

PRINCETON UNIVERSITY 1986-1997

- 1995 ASME Spirit of St. Louis Medal
- 1995 Fellow of the Royal Society of London
- 1993 American Institute of Aeronautics and Astronautics Fluid Dynamics Award
- 1990 Honorary Fellow of Trinity Hall, Cambridge
- 1990 Fellow of the American Institute of Aeronautics and Astronautics
- 1988 Gold Medal of the Royal Aeronautical Society
- 1986 Honorary Professor of Northwestern Polytechnical University, Xian, China

Stanford University



- Thomas V. Jones Professor of Engineering, 1997-Present

STANFORD UNIVERSITY 1997-PRESENT

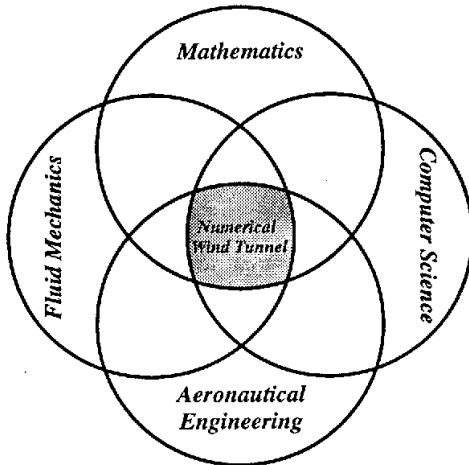
- 2006 Elmer A. Sperry Award for Advancing the Art of Transportation
- 2005 Fellow of The Royal Academy of Engineering
- 2004 Fellow of The Royal Aeronautical Society
- 2002 Docteur Honoris Causa, Uppsala University
- 2001 Docteur Honoris Causa, Universit Pierre et Marie Curie, Paris VI
- 1997 Foreign Associate, National Academy of Engineering

CFD APPLICATIONS AT BOEING AND AIRBUS

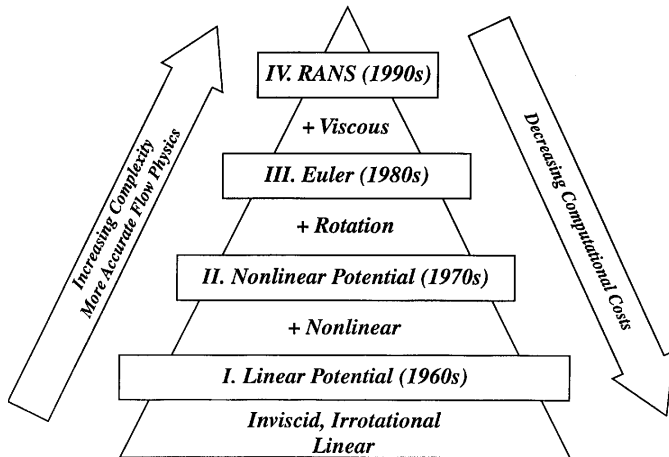
Emergence of CFD

- In 1960 the underlying principles of fluid dynamics and the formulation of the governing equations (potential flow, Euler, RANS) were well established.
- The new element was the emergence of powerful enough computers to make numerical solution possible –to carry this out required new algorithms.
- The emergence of CFD in the 1965–2005 period depended on a combination of advances in computer power and algorithms.

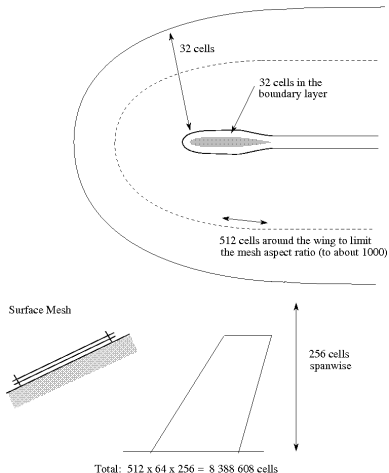
Multi-disciplinary nature of CFD



Hierarchy of CFD Equations



Computation Mesh

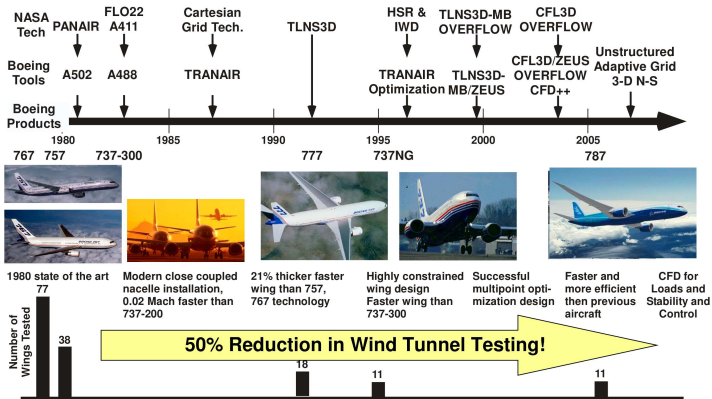


Advances in Computer Power

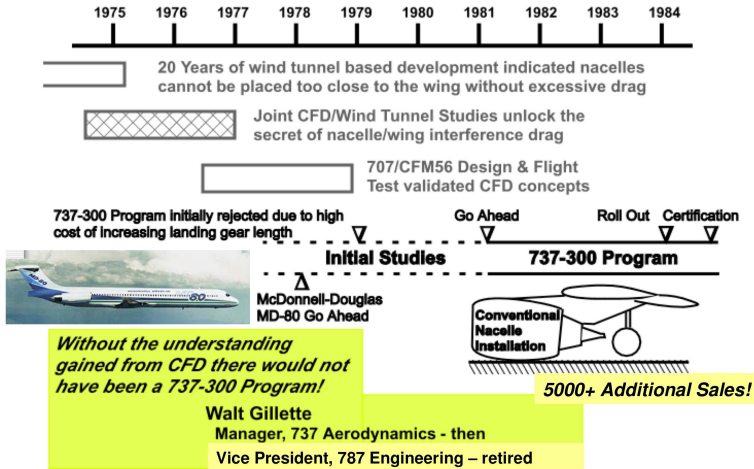
1970	CFD 6600	1	Megaflops	10^6
1980	Cray 1 vector computer	100	Megaflops	10^8
1994	IBM SP2 parallel computer	10	Gigaflops	10^{10}
2007	Linux clusters	100	Teraflops	10^{14}
2007	(affordable) BoxCluster in my house Four 3 GHz dual core CPUs (24 Gigaflops peak) \$10,000	5	Gigaflops	5×10^9
2009	HP Pavilion quadcore Notebook \$1,099	1	Gigaflops	1×10^9

CFD AT BOEING

The Impact of CFD on Configuration Lines and Wind Tunnel Testing



Impact of CFD on B737-300 Program



CFD Contributions to B787



Computational Methods at Boeing

TRANAIR

- Full Potential with directly coupled Boundary Layer**
- Cartesian solution adaptive grid**
- Drela lag-dissipation turbulence model**
- Multi-point design/optimization**

Navier-Stokes Codes

- CFL3D – Structured Multiblock Grid**
- TLNS3D - Structured Multiblock Grid - Thin Layer**
- OVERFLOW – Overset Grid**

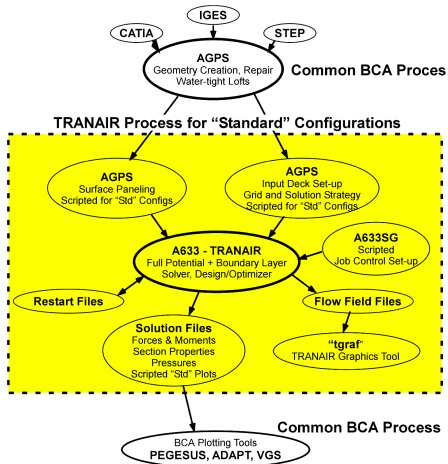
N-S Turbulence Models

- S-A Spalart-Allmaras**
- Menter's k-w SST**

Stable and Packaged Software Solution - Tranair

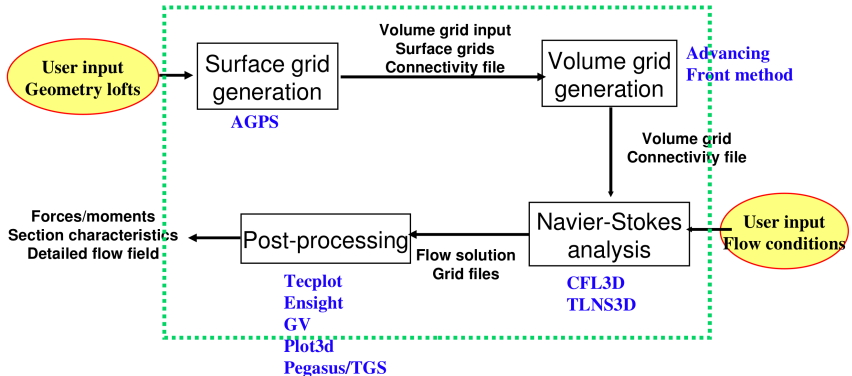
Scripted and Packaged for a “Standard” Class of Configurations

- Integral part of the engineering process
- Reduces solution flowtime
- Improves consistency and repeatability of results
- Uses common BCA processes
- Improves productivity

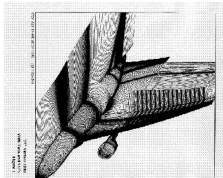


Stable and Packaged Software Solution - Zeus/CFL3D

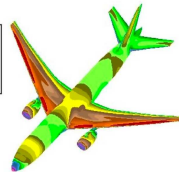
Driver for Surface Grid Generation, Volume Grid Generation, Navier-Stokes Analysis, and Post-processing



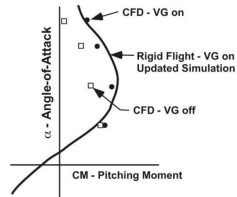
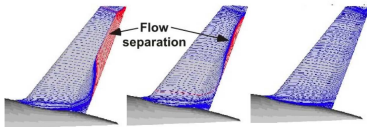
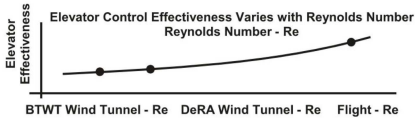
CFD for Full Flight Envelope



Computational Simulations of a transport with 16 Vortex Generators per Wing



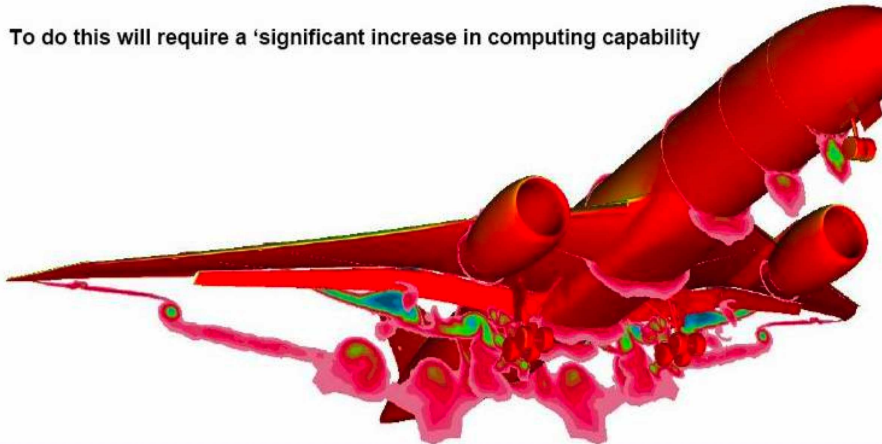
Effect of Vortex Generators on Pitching Moment at High Mach



TLNS3DMB - Multi-block Navier-Stokes
 21 Million grid points in 79 blocks
 60 CPU's - Origin 2000

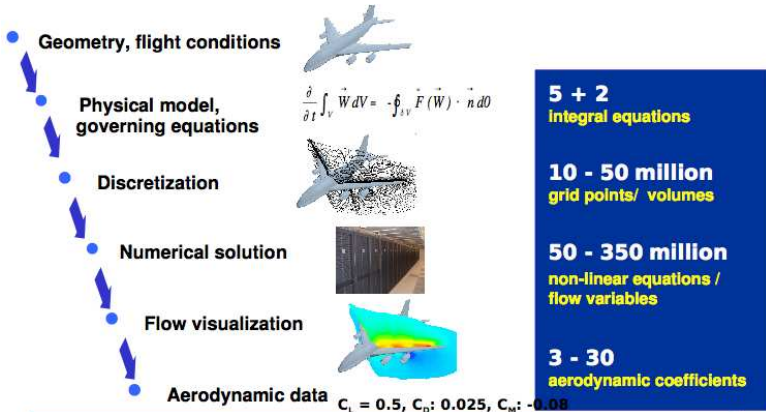
21st Century Challenge - Aeroacoustic

To do this will require a 'significant increase in computing capability



CFD AT AIRBUS AND GERMAN AEROSPACE

Numerical Flow Simulation



Problem: Quality \Leftrightarrow Accuracy \Leftrightarrow Problem Size \Leftrightarrow Time/Costs

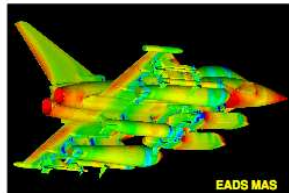
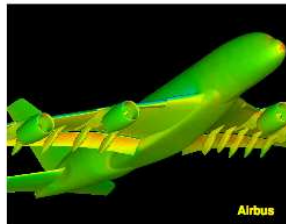
CFD Development for Aircraft Development

MEGAFLOW / MEGADESIGN

- National CFD Initiative (since 1995)

Development & validation of a **national CFD software** for complete aircraft applications which

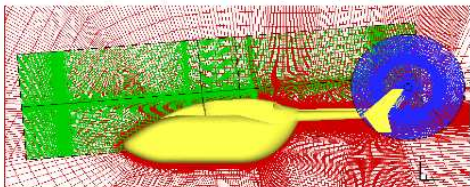
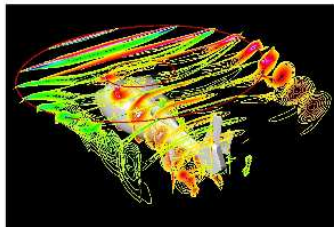
- allows computational aerodynamic analysis for 3D complex configurations at cruise, high-lift & off-design conditions
- builds the basis for shape optimization and multidisciplinary simulation
- establishes numerical flow simulation as a routinely used tool at DLR and in German aircraft industry
- serves as a development platform for universities



Block-Structured RANS Capability FLOWer

Efficient simulation tool for configurations of moderate complexity

- advanced turbulence and transition models (RSM, DES)
- state-of-the-art algorithms
 - baseline: JST scheme, multigrid
 - robust integration of RSM (DDADI)
- chimera technique for moving bodies
- fluid / structure coupling
- design option (inverse design, adjoint)



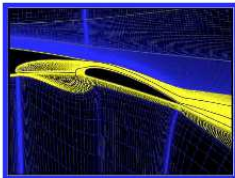
FLOWer-Code

- Fortran
- portable code
- parallelization based on MPI

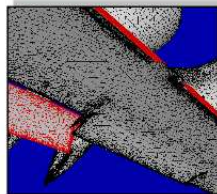
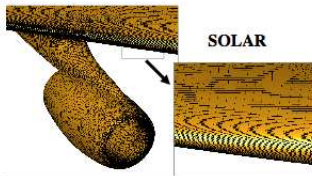
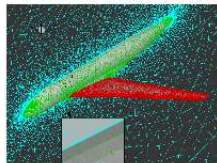
Mesh Generation

Tools

- **structured grids**
 - *DLR MegaCads*
 - *ICEM-Hexa*
- **unstructured grids**
 - *CENTAUR*,
 - *UK SOLAR mesher*
 - *EADS-M mesher*
- **structured/unstructured grids**
 - *DLR MegaCads*



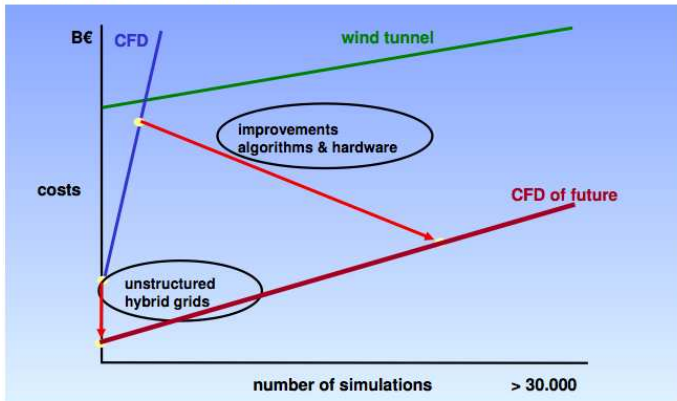
MegaCads



Centaur

Numerical Flow Simulation

Relation CFD / wind tunnel



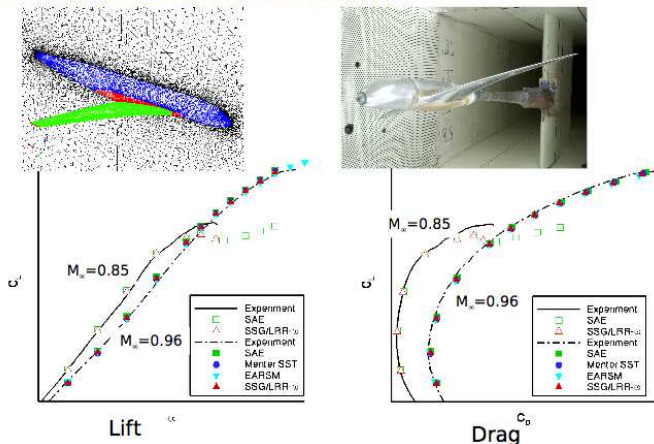
✈️ **CFD cost effective alternative**

CFD Contribution to A380



Cruise Configuration

Influence of Mach number and incidence



Aircraft at High Lift Configuration

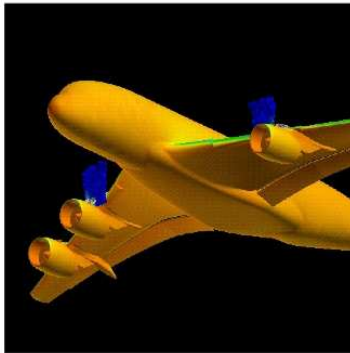
Effect of nacelle strakes on civil transport configuration



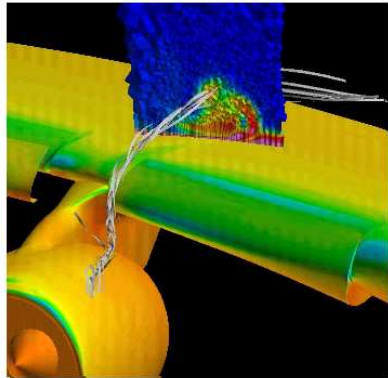
Aircraft at High Lift Configuration

Effect of nacelle strakes on civil transport configuration

- detailed CFD investigation using CFD (DLR TAU-Code)



hybrid grid: 17 million points, 3x adapted



$M=0.18$. $Re=3 \times 10^6$

FLO AND SYN CODES AND THEIR USAGES

FLO and SYN Codes

This series of codes has been developed since 1970 for progressively more complex models of fluid flow, more complex geometric configurations, and more advanced algorithms.

FLO Code I

- 1970, flo 1, 2, solution of 2D potential flow by conformal mapping
- 1971-3, flo 6, 2D transonic potential flow (rotated difference scheme)
- 1975, flo 22, first transonic potential flow solution for a swept wing (co-author D. Caughey) -first used for the wing design of the Canadair Challenger, later marketed as XFLO 22 by the Dutch NLR, still in use today at Boeing, Long Beach
- 1977, flo 27, 3D potential flow in general grid with trilinear isoparametric elements (incorporated in Boeing A488 software)

FLO Code II

- 1979, flo 36, multigrid solution of 2D transonic potential flow in 3-10 (.06 sec. on IBM T30 laptop)
- 1981, flo 57, solution of 3D Euler equations, - used worldwide; derivatives include NASA's TLNS3D, Lockheed's TEAM code, British Aerospace's codes EJ30, EJ65, Dornier Ikarus code
- 1983, flo 82, multigrid solution of 2D Euler Equations in 25-50 steps
- 1985, flo 67, multigrid solution of 3D Euler equations in 25-50 steps
- 1988, flo 97, 107, cell-vertex and cell-centered schemes for 3D Navier-Stokes equations
- 1991, uflo 82, 87, dual timestepping scheme for unsteady flow - used in Tflo code for Stanford's ASCI project

FLO Code III

- 2001, flo 82-sgs "textbook" multigrid solution of 2D and 3D Euler equations flo 88-sgs 3-5 steps with nonlinear symmetric Gauss-Seidel scheme
- 2003, flo-3xx, viscous flow solution on arbitrary polyhedral meshes

SYN Code

- 1970, syn 1, solution of inverse problem by conformal mapping (Lighthill's method)
- 1989, syn 36, airfoil design in transonic potential flow via control theory
- 1993-5, syn 87, 88, wing design by control theory using 3D Euler equations
- 1997, syn 107, wing design by control theory using 3D Navier-Stokes equations
- 2003, syn-3xx, aerodynamic design of general configurations in viscous flow on arbitrary meshes

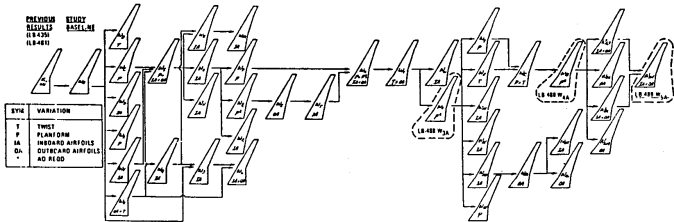
AIRPLANE Code

- 1985, airplane, first solution of Euler equations for a complete aircraft (tetrahedral mesh) used by McDonald Douglas (MD 11), NASA (HSCT), Mitsubishi, EADS (basis of their current software Airplane+)
- 2003, synplane, aerodynamic design of complete aircraft using control theory with tetrahedral mesh

CALCULATIONS USING FLO22 CODE

Wing Configuration Matrix Evaluated

AERODYNAMIC DEVELOPMENT WING CONFIGURATION MATRIX EVALUATED WITH THE 3-D DOUGLAS-JAMESON TRANSONIC PROGRAM



**WINGS SELECTED FOR WIND TUNNEL TESTING
 IN AMES II FT FACILITY**

8-DC10-10700A

CALCULATIONS USING FLO57 CODE

Northrop YF23

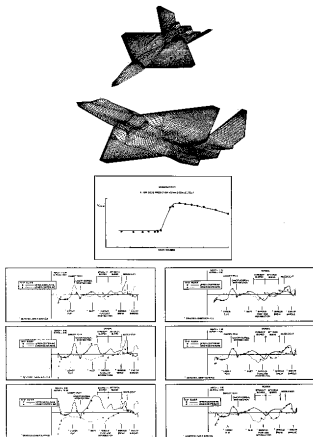
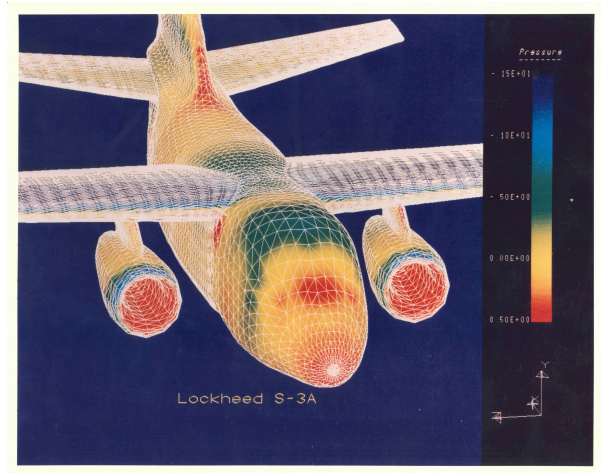


Plate 1: Northrop YF-23.
Supplied by R.J. Bush, Jr.

CALCULATIONS USING AIRPLANE CODE

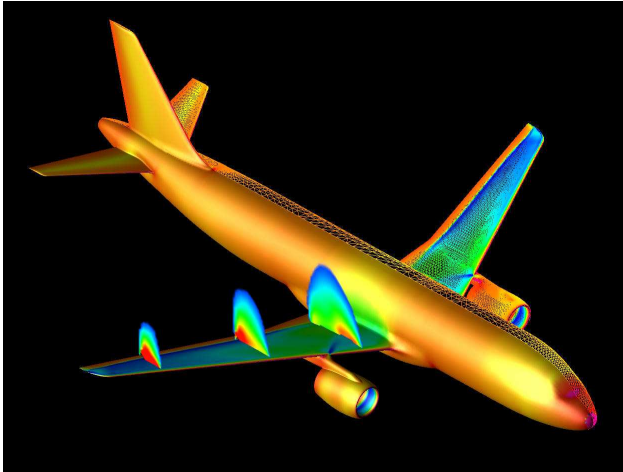
Lockheed S-3A



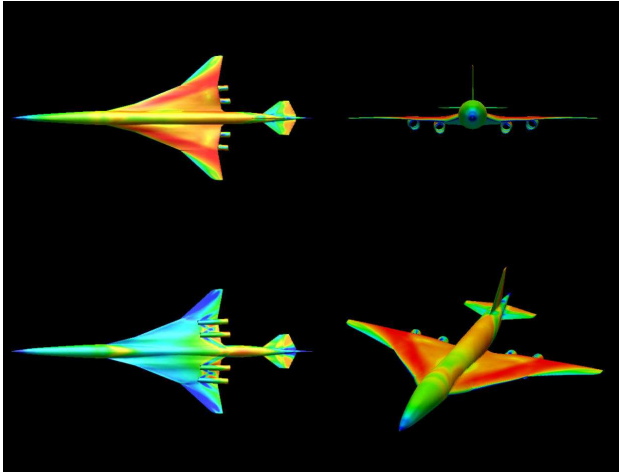
McDonnell Douglas MD11



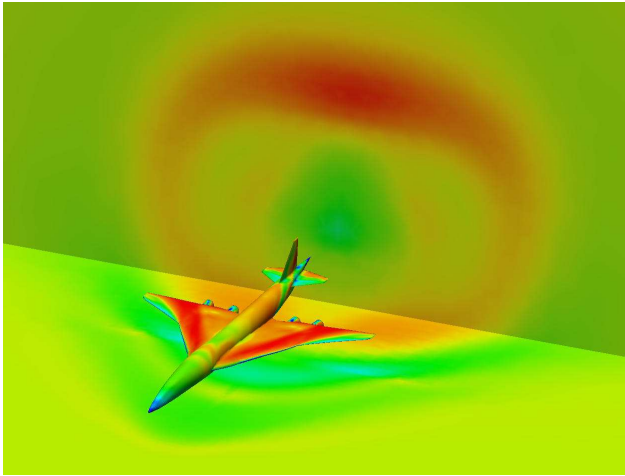
Airbus A320



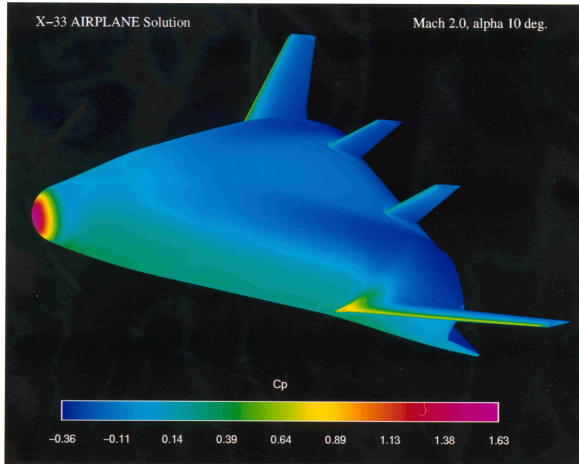
Supersonic Transport



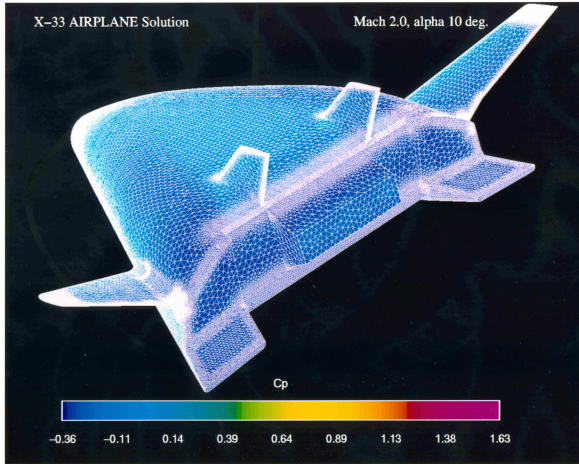
Supersonic Transport



X33



X33



RANS CALCULATIONS USING FLO97MB AND FLO107MB

Navier–Stokes Simulation of the MAGLEV Train

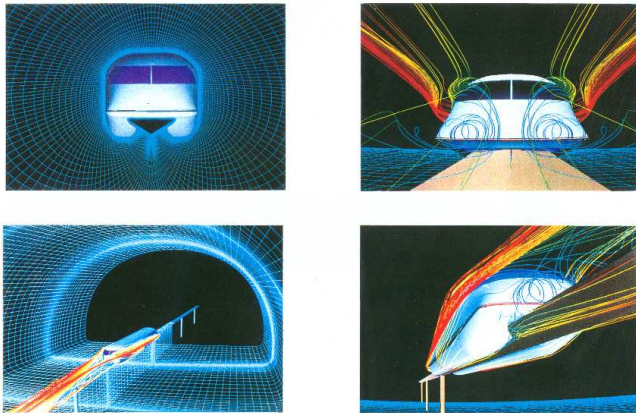


Plate 12: Navier-Stokes Simulation of the MAGLEV Train,
Supplied by M.J. Siclari.

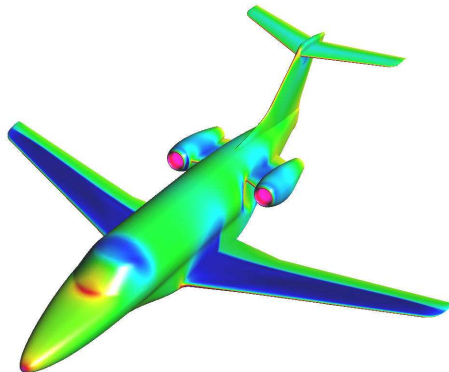
Beechcraft Aircraft

Transonic Business Jet

FLO107-MB Solution

Baldwin-Lomax Turbulence Model

Mach = .82 240 Blocks 5.8 Million Mesh Points



Usage of FLO and SYN Code I

The "flo" series of codes has been used worldwide in the design of many aircrafts. These include:

- Airbus
- Boeing
- Canadair
- McDonnell Douglas
- Northrop
- Beech
- Embraer
- Gulfstream

Usage of FLO Code I

- Airbus
 - ① 310 (flo 57 derivatives EJ30, EJ65)
 - ② 320 (flo 57 derivatives EJ30, EJ65)
 - ③ 330 (flo 57 derivatives EJ30, EJ65)
 - ④ 340 (flo 57 derivatives EJ30, EJ65)
- Boeing
 - ① 737-500 (flo 27-28 incorporated in Boeing A488 software)
 - ② 747-400 (flo 27-28 incorporated in Boeing A488 software)
 - ③ 757 (flo 27-28 incorporated in Boeing A488 software)
 - ④ 767 (flo 27-28 incorporated in Boeing A488 software)
 - ⑤ 777 (flo 27-28 incorporated in Boeing A488 software)
- Canadair
 - ① Challenger (flo 22)
 - ② Regional Jet (flo 22)

Usage of FLO Code II

- Hermes
 - ① spaceplane (flo 57 derivative Ikarus)
- McDonnell Douglas
 - ① C17 (flo 22)
 - ② MD11 (flo 22, airplane)
 - ③ MD12 (flo 67, airplane)
 - ④ MDXX (syn 88)
 - ⑤ MDHSCT (flo 67, airplane)
 - ⑥ MD90 (flo 27 incorporated in dactran10)
 - ⑦ MD95: later Boeing 717 (flo 22, flo 67)
- Northrop
 - ① B2 (flo 22)
 - ② F23 (flo 57)

Usage of SYN and Airplane Code I

- Airbus
 - ① 380 (syn 88)
- Beech
 - ① Premier (syn 87 MB)
 - ② Horizon (syn 87 MB)
- Embraer
 - ① 190 (syn 88)
- Gulfstream
 - ① G650 (syn 107)
- McDonnell Douglas
 - ① MD11 (airplane)
 - ② MD12 (airplane)
 - ③ MDXX (syn 88)
 - ④ MDHSCT (airplane)

Sperry Award



The Elmer A. Sperry Award

The Elmer A. Sperry Award shall be given in recognition of a distinguished engineering contribution which, through application, proved in actual service, has advanced the art of transportation whether by land, sea or air.

In the words of Edmondo Quattrocchi, sculptor of the Elmer A. Sperry Medal:

"This Sperry medal symbolizes the struggle of man's mind against the forces of nature.

The horse represents the primitive state of uncontrolled power. This, as suggested by the clouds and celestial fragments, is essentially the same in all the elements. The Gyroscope, superimposed on these, represents the bringing of this power under control for man's purposes."

Presentation of
The Elmer A. Sperry Award
for 2006

to

ANTONY JAMESON

in recognition of his seminal and continuing contributions to the modern design of aircraft through his numerous algorithmic innovations and through the development of the FLO, SYN, and AIRPLANE series of computational fluid dynamics codes.

by

The Elmer A. Sperry Board of Award
under the sponsorship of the:

American Society of Mechanical Engineers
Institute of Electrical and Electronics Engineers
Society of Automotive Engineers
Society of Naval Architects and Marine Engineers
American Institute of Aeronautics and Astronautics
American Society of Civil Engineers

at the
45th AIAA Aerospace Sciences Meeting and Exhibit
Reno, Nevada

9 January 2007

Flo and Syn Codes

CODES		AIRPLANES	
1970	FLO1, 2 SYN1	Canadair	Challenger (FLO 22) Regional Jet (FLO 22) Global Express (airplane)
1971-1973	FLO 6	Northrop	B2 (FLO 22) F23 (FLO 57)
1975	FLO 22	Boeing	737-500 (FLO 27-28 incorporated in Boeing A488 software) 747-400 (FLO 27-28 incorporated in Boeing A488 software) 757 (FLO 27-28 incorporated in Boeing A488 software) 767 (FLO 27-28 incorporated in Boeing A488 software) 777 (FLO 27-28 incorporated in Boeing A488 software) 787 (FLO 27-28 incorporated in Boeing A488 software)
1977	FLO 27	McDonnell-Douglas	C17 (FLO 22) MD11 (FLO 22, airplane) MD12 (FLO 67, airplane) MDXX (SYN 88) MDHSC1 (FLO 67, airplane) MD90 (FLO 27 incorporated in dactran10) MD95: later Boeing 717 (FLO 22, FLO 67)
1979	FLO 36	Airbus	310 (FLO 57 derivatives EJ30, EJ65) 320 (FLO 57 derivatives EJ30, EJ65) 330 (FLO 57 derivatives EJ30, EJ65) 340 (FLO57 derivatives EJ30, EJ65) 380 (SYN 88)
1981	FLO 52, 57	Beech	Premier (SYN 87 MB) Horizon (SYN 87 MB)
1984	FLO 62, 67	Embraer	190 (SYN 88)
1985	AIRPLANE		
1985	FLO 82, 87		
1988	FLO 97, 107		
1989	SYN 36		
1991	UFLO 82, 87		
1993-1995	SYN 87, 88		
1997	SYN 107		
2001	FLO 82-SGS FLO 88-SGS		
2003	SYNPLANE		
2003-2006	FLO-3xx SYN-3xx		

The Boeing Airplanes that have Benefited from Antony Jameson's CFD Technology



MATHEMATICS OF ADJOINT BASED SHAPE OPTIMIZATION

DESIGN USING THE EULER EQUATIONS

Design using the Euler Equations

In a fixed computational domain with coordinates, ξ , the Euler equations are

$$J \frac{\partial w}{\partial t} + R(w) = 0 \quad (9)$$

where J is the Jacobian (cell volume),

$$R(w) = \frac{\partial}{\partial \xi_i} (S_{ij} f_j) = \frac{\partial F_i}{\partial \xi_i}. \quad (10)$$

and S_{ij} are the metric coefficients (face normals in a finite volume scheme). We can write the fluxes in terms of the scaled contravariant velocity components

$$U_i = S_{ij} u_j$$

as

$$F_i = S_{ij} f_j = \begin{bmatrix} \rho U_i \\ \rho U_i u_1 + S_{i1} p \\ \rho U_i u_2 + S_{i2} p \\ \rho U_i u_3 + S_{i3} p \\ \rho U_i H \end{bmatrix}.$$

where $p = (\gamma - 1)\rho(E - \frac{1}{2}u_i^2)$ and $\rho H = \rho E + p$.

Design using the Euler Equations

For simplicity, it will be assumed that the portion of the boundary that undergoes shape modifications is restricted to the coordinate surface $\xi_2 = 0$. Then equations for the variation of the cost function and the adjoint boundary conditions may be simplified by incorporating the conditions

$$n_1 = n_3 = 0, \quad n_2 = 1, \quad \mathcal{B}_\xi = d\xi_1 d\xi_3,$$

so that only the variation δF_2 needs to be considered at the wall boundary. The condition that there is no flow through the wall boundary at $\xi_2 = 0$ is equivalent to

$$U_2 = 0, \quad \text{so that} \quad \delta U_2 = 0$$

when the boundary shape is modified. Consequently the variation of the inviscid flux at the boundary reduces to

$$\delta F_2 = \delta p \begin{Bmatrix} 0 \\ S_{21} \\ S_{22} \\ S_{23} \\ 0 \end{Bmatrix} + p \begin{Bmatrix} 0 \\ \delta S_{21} \\ \delta S_{22} \\ \delta S_{23} \\ 0 \end{Bmatrix}. \quad (13)$$

Design using the Euler Equations

In order to design a shape which will lead to a desired pressure distribution, a natural choice is to set

$$I = \frac{1}{2} \int_B (p - p_d)^2 dS$$

where p_d is the desired surface pressure, and the integral is evaluated over the actual surface area. In the computational domain this is transformed to

$$I = \frac{1}{2} \iint_{B_w} (p - p_d)^2 |S_2| d\xi_1 d\xi_3,$$

where the quantity

$$|S_2| = \sqrt{S_{2j} S_{2j}}$$

denotes the face area corresponding to a unit element of face area in the computational domain.

Design using the Euler Equations

In the computational domain the adjoint equation assumes the form

$$C_i^T \frac{\partial \psi}{\partial \xi_i} = 0 \quad (14)$$

where

$$C_i = S_{ij} \frac{\partial f_j}{\partial w}.$$

To cancel the dependence of the boundary integral on δp , the adjoint boundary condition reduces to

$$\psi_j n_j = p - p_d \quad (15)$$

where n_j are the components of the surface normal

$$n_j = \frac{S_{2j}}{|S_2|}.$$

Design using the Euler Equations

This amounts to a transpiration boundary condition on the co-state variables corresponding to the momentum components. Note that it imposes no restriction on the tangential component of ψ at the boundary.

We find finally that

$$\delta I = - \int_{\mathcal{D}} \frac{\partial \psi^T}{\partial \xi_i} \delta S_{ij} f_j d\mathcal{D} - \iint_{B_W} (\delta S_{21} \psi_2 + \delta S_{22} \psi_3 + \delta S_{23} \psi_4) p d\xi_1 d\xi_3. \quad (16)$$

Here the expression for the cost variation depends on the mesh variations throughout the domain which appear in the field integral. However, the true gradient for a shape variation should not depend on the way in which the mesh is deformed, but only on the true flow solution. In the next section we show how the field integral can be eliminated to produce a reduced gradient formula which depends only on the boundary movement.

The Reduced Gradient Formulation

Consider the case of a mesh variation with a fixed boundary. Then $\delta I = 0$ but there is a variation in the transformed flux,

$$\delta F_i = C_i \delta w + \delta S_{ij} f_j.$$

Here the true solution is unchanged. Thus, the variation δw is due to the mesh movement δx at each mesh point. Therefore

$$\delta w = \nabla w \cdot \delta x = \frac{\partial w}{\partial x_j} \delta x_j (= \delta w^*)$$

and since $\frac{\partial}{\partial \xi_i} \delta F_i = 0$, it follows that

$$\frac{\partial}{\partial \xi_i} (\delta S_{ij} f_j) = - \frac{\partial}{\partial \xi_i} (C_i \delta w^*). \quad (17)$$

It has been verified by Jameson and Kim[★] that this relation holds in the general case with boundary movement.

★ "Reduction of the Adjoint Gradient Formula in the Continuous Limit", A. Jameson and S. Kim, 41st AIAA Aerospace Sciences Meeting & Exhibit, AIAA Paper 2003-0040, Reno, NV, January 6-9, 2003.

VISCOUS ADJOINT TERMS

Derivation of the Viscous Adjoint Terms

The viscous terms will be derived under the assumption that the viscosity and heat conduction coefficients μ and k are essentially independent of the flow, and that their variations may be neglected. This simplification has been successfully used for many aerodynamic problems of interest. In the case of some turbulent flows, there is the possibility that the flow variations could result in significant changes in the turbulent viscosity, and it may then be necessary to account for its variation in the calculation.

Transformation to Primitive Variables

The derivation of the viscous adjoint terms is simplified by transforming to the primitive variables

$$\tilde{w}^T = (\rho, u_1, u_2, u_3, p)^T,$$

because the viscous stresses depend on the velocity derivatives $\frac{\partial U_i}{\partial x_j}$, while the heat flux can be expressed as

$$\kappa \frac{\partial}{\partial x_i} \left(\frac{p}{\rho} \right).$$

where $\kappa = \frac{k}{R} = \frac{\gamma \mu}{Pr(\gamma-1)}$. The relationship between the conservative and primitive variations is defined by the expressions

$$\delta w = M \delta \tilde{w}, \quad \delta \tilde{w} = M^{-1} \delta w$$

which make use of the transformation matrices $M = \frac{\partial w}{\partial \tilde{w}}$ and $M^{-1} = \frac{\partial \tilde{w}}{\partial w}$

Transformation to Primitive Variables

These matrices are provided in transposed form for future convenience

$$M^T = \begin{bmatrix} 1 & u_1 & u_2 & u_3 & \frac{u_i u_j}{2} \\ 0 & \rho & 0 & 0 & \rho u_1 \\ 0 & 0 & \rho & 0 & \rho u_2 \\ 0 & 0 & 0 & \rho & \rho u_3 \\ 0 & 0 & 0 & 0 & \frac{1}{\gamma-1} \end{bmatrix}$$

$$M^{-1T} = \begin{bmatrix} 1 & -\frac{u_1}{\rho} & -\frac{u_2}{\rho} & -\frac{u_3}{\rho} & \frac{(\gamma-1)u_i u_j}{2} \\ 0 & \frac{1}{\rho} & 0 & 0 & -(\gamma-1)u_1 \\ 0 & 0 & \frac{1}{\rho} & 0 & -(\gamma-1)u_2 \\ 0 & 0 & 0 & \frac{1}{\rho} & -(\gamma-1)u_3 \\ 0 & 0 & 0 & 0 & \gamma-1 \end{bmatrix} .$$

The Viscous Adjoint Field Operator

Collecting together the contributions from the momentum and energy equations, the viscous adjoint operator in primitive variables can be expressed as

$$\begin{aligned}
 (\tilde{L}\psi)_1 &= -\frac{\rho}{\rho^2} \frac{\partial}{\partial \xi_l} \left(S_{lj} \kappa \frac{\partial \theta}{\partial x_j} \right) \\
 (\tilde{L}\psi)_{i+1} &= \frac{\partial}{\partial \xi_l} \left\{ S_{lj} \left[\mu \left(\frac{\partial \phi_i}{\partial x_j} + \frac{\partial \phi_j}{\partial x_i} \right) + \lambda \delta_{ij} \frac{\partial \phi_k}{\partial x_k} \right] \right\} \\
 &\quad + \frac{\partial}{\partial \xi_l} \left\{ S_{lj} \left[\mu \left(u_i \frac{\partial \theta}{\partial x_j} + u_j \frac{\partial \theta}{\partial x_i} \right) + \lambda \delta_{ij} u_k \frac{\partial \theta}{\partial x_k} \right] \right\} \\
 &\quad - \sigma_{ij} \left(S_{lj} \frac{\partial \theta}{\partial x_j} \right) \\
 (\tilde{L}\psi)_5 &= \frac{1}{\rho} \frac{\partial}{\partial \xi_l} \left(S_{lj} \kappa \frac{\partial \theta}{\partial x_j} \right).
 \end{aligned}$$

The conservative viscous adjoint operator may now be obtained by the transformation

$$L = M^{-1T} \tilde{L}$$

Viscous Adjoint Boundary Conditions

The boundary conditions satisfied by the flow equations restrict the form of the performance measure that may be chosen for the cost function. There must be a direct correspondence between the flow variables for which variations appear in the variation of the cost function, and those variables for which variations appear in the boundary terms arising during the derivation of the adjoint field equations. Otherwise it would be impossible to eliminate the dependence of δI on δw through proper specification of the adjoint boundary condition. In fact it proves that it is possible to treat any performance measure based on surface pressure and stresses such as the force coefficients, or an inverse problem for a specified target pressure.

SOBOLEV INNER PRODUCT

The Need for a Sobolev Inner Product in the Definition of the Gradient

Another key issue for successful implementation of the continuous adjoint method is the choice of an appropriate inner product for the definition of the gradient. It turns out that there is an enormous benefit from the use of a modified Sobolev gradient, which enables the generation of a sequence of smooth shapes. This can be illustrated by considering the simplest case of a problem in the calculus of variations. Suppose that we wish to find the path $y(x)$ which minimizes

$$I = \int_a^b F(y, y') dx$$

with fixed end points $y(a)$ and $y(b)$.
 Under a variation $\delta y(x)$,

$$\begin{aligned} \delta I &= \int_a^b \left(\frac{\partial F}{\partial y} \delta y + \frac{\partial F}{\partial y'} \delta y' \right) dx \\ &= \int_a^b \left(\frac{\partial F}{\partial y} - \frac{d}{dx} \frac{\partial F}{\partial y'} \right) \delta y dx \end{aligned}$$

The Need for a Sobolev Inner Product in the Definition of the Gradient

Thus defining the gradient as

$$g = \frac{\partial F}{\partial y} - \frac{d}{dx} \frac{\partial F}{\partial y'}$$

and the inner product as

$$(u, v) = \int_a^b u v dx$$

we find that

$$\delta I = (g, \delta y).$$

If we now set

$$\delta y = -\lambda g, \quad \lambda > 0,$$

we obtain an improvement

$$\delta I = -\lambda (g, g) \leq 0$$

unless $g = 0$, the necessary condition for a minimum.

The Need for a Sobolev Inner Product in the Definition of the Gradient

Note that g is a function of y, y', y'' ,

$$g = g(y, y', y'')$$

In the well known case of the Brachistrone problem, for example, which calls for the determination of the path of quickest descent between two laterally separated points when a particle falls under gravity,

$$F(y, y') = \sqrt{\frac{1 + y'^2}{y}}$$

and

$$g = -\frac{1 + y'^2 + 2yy''}{2[y(1 + y'^2)]^{3/2}}$$

It can be seen that each step

$$y^{n+1} = y^n - \lambda^n g^n$$

reduces the smoothness of y by two classes. Thus the computed trajectory becomes less and less smooth, leading to instability.

The Need for a Sobolev Inner Product in the Definition of the Gradient

In order to prevent this we can introduce a weighted Sobolev inner product

$$\langle u, v \rangle = \int (uv + \epsilon u' v') dx$$

where ϵ is a parameter that controls the weight of the derivatives. We now define a gradient \bar{g} such that $\delta I = \langle \bar{g}, \delta y \rangle$. Then we have

$$\begin{aligned} \delta I &= \int (\bar{g} \delta y + \epsilon \bar{g}' \delta y') dx \\ &= \int \left(\bar{g} - \frac{\partial}{\partial x} \epsilon \frac{\partial \bar{g}}{\partial x} \right) \delta y dx \\ &= (g, \delta y) \end{aligned}$$

where

$$\bar{g} - \frac{\partial}{\partial x} \epsilon \frac{\partial \bar{g}}{\partial x} = g$$

and $\bar{g} = 0$ at the end points.

The Need for a Sobolev Inner Product in the Definition of the Gradient

Therefore \bar{g} can be obtained from g by a smoothing equation.
Now the step

$$y^{n+1} = y^n - \lambda^n \bar{g}^n$$

gives an improvement

$$\delta I = -\lambda^n \langle \bar{g}^n, \bar{g}^n \rangle$$

but y^{n+1} has the same smoothness as y^n , resulting in a stable process.